X-Ray Absorption Spectroscopy Imaging of Biological Tissues

Ingrid J. Pickering and Graham N. George

Department of Geological Sciences, University of Saskatchewan,
114 Science Place, Saskatoon, SK, S7N 4R5 Canada

Abstract. X-ray absorption spectroscopy (XAS) is proving invaluable in determining the average chemical form of metals or metalloids in intact biological tissues. As most tissues have spatial structure, there is great additional interest in visualizing the spatial location of the metal(loid) as well as its chemical forms. XAS imaging gives the opportunity of producing maps of specific chemical types of elements *in vivo* in dilute biological systems. X-ray fluorescence microprobe techniques are routinely used to study samples with spatial heterogeneity. Microprobe produces elemental maps, with chemical sensitivity obtained by recording micro-XAS spectra at selected point locations on the map. Unfortunately, using these procedures spatial detail may be lost as the number of point spectra recorded generally is limited. A powerful extension of microprobe is XAS imaging or chemically specific imaging. Here, the incident energy is tuned to features in the near-edge which are characteristic of the expected chemical forms of the element. With a few simple assumptions, these XAS images can then be converted to quantitative images of specific chemical form, yielding considerable clarity in the distributions.

Keywords: X-ray absorption spectroscopy imaging; biological tissues; microprobe; fern; arsenic; *Pteris vittata*.
PACS: 82.80.Ej; 87.59.-e; 87.64.Gb; 89.60.-k; 87.14.-g

INTRODUCTION

X-ray absorption spectroscopy (XAS) is proving to be a unique *in situ* probe of metals or metalloids in biological materials [1]. XAS can target the element of interest and yield average chemical information from biological tissues essentially without pretreatment. XAS can detect metals in any state of matter (solid, dissolved aqueous, gaseous, etc.). Its ability to yield an average picture of the molecular form of a metal within a complex specimen makes it particularly useful for biological materials. Such materials can range from isolated subcellular components such as lysosomes, through cell cultures and intact tissues to whole (small) organisms.

Most biological materials are by their nature structured, so in addition to determining the average chemical form of an element in a biological sample, we would also like to obtain spatial information. Is the element diffusely distributed, or specifically localized in special organelles, cells, or organs (depending on the length scale)? We would like to know where within the structure the element is localized and whether it is co-localized with other elements. If more than one chemical form is present, we would additionally like to know how each of these species is distributed.

Simultaneous Chemical and Spatial Information: Two Contrasting Methods

Here we will consider two methods for obtaining information on the distribution of dilute chemical species in a structured sample.

a. μ-XRF and μ-XAS

This commonly-employed method uses micro-X-ray fluorescence (μ-XRF) to produce an elemental map. Once the map is completed, pixels of interest are selected and μ-XAS spectra are collected to determine the chemical form. The advantages of this method are i) the sample need only be rastered once; ii) no previous knowledge about chemical forms and the XAS spectra thereof are required; iii) at each individual pixel, the chemical information provided by the complete spectrum is more definitive. The major disadvantage is that chemical information is only determined at isolated pixels, and in doing so some detail of the complete picture may be lost. An

additional disadvantage for biological materials is that beam damage issues may be more problematic, as will be discussed below.

b. XAS Imaging

In X-ray absorption spectroscopy imaging (XAS imaging, also called XANES imaging or image stacks), the incident energy is tuned to spectroscopic features in the near-edge to provide contrast between two or more chemical species present in the specimen [2] (Fig. 1). This requires rastering the sample multiple times (so greater image data collection time) and a pre-knowledge of the chemical forms in the sample. However, the main advantage is that complete maps of the chemical forms can be derived, sometimes revealing details which would remain hidden using μ-XRF and μ-XAS. Additionally, irradiation durations and the elapsed time between the start and completion of data collection for each pixel are significantly reduced, with benefits for biological materials as will be discussed in the next section.

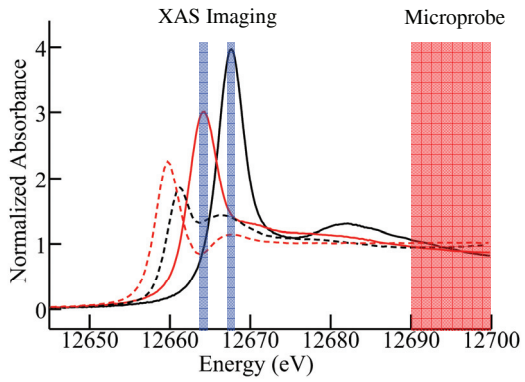

FIGURE 1. Energies for microprobe vs. XAS imaging. Microprobe is conducted with the energy well above the absorption edge (typically even higher than is indicated here). In XAS imaging, energies are tuned to the features in the absorption edge. In this case (Se K-edge) the image is discriminating for selenate (highest energy) and selenite. Knowledge of the chemical forms which might be present, and stable energy calibration, is a prerequisite for this type of imaging.

EXPERIMENTAL CONSIDERATIONS

Radiation Damage Issues

As synchrotron sources and improved focusing optics produce brighter beams, radiation damage issues become more acute. Beam damage effects are of especial concern for delicate biological tissues. The effects of radiation damage are complex, depending on many factors including the nature of the sample, energy of the X-rays, dose, and time elapsed since irradiation. Effects of radiation damage can vary from subtle changes in spectra to, in extreme cases, total sample destruction.

Monitoring the Effects of Radiation

In our work we have employed at least three methods of monitoring whether there is perceptible radiation damage.

i) Spectral changes. Changes in the X-ray absorption spectrum are a very sensitive monitor of sample integrity. If replicate spectra show changes, then the sample is changing. Unfortunately, if replicate spectra are identical, this means that either beam damage is negligible, or the changes happened before the spectrum could be measured.

ii) Visual inspection. Visible changes such as variations in color, shape, morphology of cells, and so on are an indication that beam damage has occurred.

iii) External tests of sample integrity. In the Trypan Blue test, a blue dye is administered to an animal cell culture. While all cells take up the dye, healthy cells actively pump the dye out and appear colorless whereas unhealthy cells retain it and are stained blue.

Minimizing Radiation Effects in the Data

Minimizing effects in the data include i) Preserving the sample (freeze drying, cryoprotecting) and ii) minimizing the dwell time at each pixel (see Fig. 2).

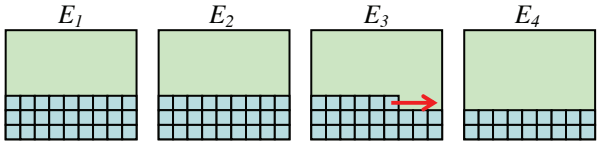

FIGURE 2. Schematic showing optimized raster scanning scheme for XAS imaging. Rather than collecting a complete image at energy E_1 before moving to E_2, a single raster is completed at all energies (E_1 to E_4 in this example). Thus, a relatively short amount of time elapses between the start and end observations of a given pixel.

Choosing the Pixel Size

Biological imaging length scales can range from the nanometer scale to as large as a moose. As the image needs to be built up pixel by pixel, the size of the pixel needs to be tuned to the question in hand. While sub-micron experiments can yield unprecedented microscopic detail, the area imaged will

be concomitantly small. A coarser image may be valuable in revealing more of the longer range, anatomical detail.

Data Collection

Data presented in this article were collected on beamline 9-3 of the Stanford Synchrotron Radiation Laboratory with a tapered metal monocapillary focusing optic [3]. Fluoresence was measured using a single element Canberra leGe detector.

Quantitative Data Analysis

Quantitative concentration maps can be extracted from fluorescence maps of soft biological materials by measurement of standards and one simple approximation [2]. The approximation is to treat the composition of the soft tissue, for the purposes of modeling the X-ray absorption, to be that of 100% water. In most cases this is either an excellent approximation, or the materials present are composed of other abundant light elements (C, N, O, H) which have similar absorption characteristics.

Data analysis of the fluorescence maps consists of the following: i) using the fluorescence signal to determine the molar amount of each component; ii) converting the absorption map to a map of effective thickness and iii) combining the amounts with the effective thickness to obtain maps of concentrations for each of the species.

Determining Molar Amounts

If these are collected using an energy dispersive detector, the contributions of scatter or fluorescence from other elements should first be removed from the signal. Scatter is more of an issue for XAS imaging than for μ-XRF because the incident energy (and therefore the elastic scatter) is lower in energy and therefore may overlap somewhat with the fluorescence line. Methods for removing the scatter from windows counts have been given previously [2].

For each pixel there is an array of (corrected) fluorescence intensities F_j corresponding to the j energies of observation. These are related to the molar quantities per pixel, m_i, for each of the i components, by:

$$F_j = k_q \sum_i m_i I_{ij} \qquad (1)$$

where I_{ij} is the normalized intensity of the standard spectrum of component i at energy j. k_q is a quantitation standard which can be determined from measuring a standard of known concentration and pathlength under the same conditions as the sample. k_q can be defined by $J_s = k_q m_s$, where J is the observed height of the edge jump for a standard s and m_s is moles per pixel for the standard. For a standard of known concentration c_s and thickness t_s, $k_q = J_s/(c_s a t_s)$ for a beam area of a. Molar quantities m_i can then be extracted from equation (1) by matrix inversion.

Deriving Effective Thickness

The measured absorption per pixel (A) derived simply from the upstream (I_0) and downstream (I_1) intensities is given by $A = \log_e(I_0/I_1)$. A includes contributions from absorption of windows, gases, etc., together with any differences in gains or responses of the detector. Luckily, simple subtraction of a background absorption (B, measured as A except no sample) results in an absorption of the sample alone. From this, the effective thickness per pixel (t) can be simply derived by using the absorption cross section (σ) and density (ρ), both assumed to be that of water (equation (2)).

$$t = \frac{(A - B)}{\sigma\rho} \qquad (2)$$

Determining Concentrations

Concentrations c_i of the components i can then be simply determined from the molar quantities m_i and the volume:

$$c_i = \frac{m_i}{at} \qquad (3)$$

RESULTS AND DISCUSSION

Results are drawn from a recent study of arsenic in the hyperaccumulating fern *Pteris vittata* [4]. This fern, discovered growing in Florida [5], has the remarkable ability to take up huge quantities of arsenate from the soil to store it in its above ground biomass. Even more remarkably, the fern appears to transform the arsenate in the soil, already a toxic species, into the even more deadly arsenite [6] for storage. The biochemistry and physiology of how the fern deals with this toxic cargo is of interest in itself. It is of practical interest also in the areas of phytoremediation or phytofiltration, and indeed this fern has already been the subject of pilot studies in these areas [7]. The XAS imaging study showcases the benefits of this technique for obtaining a more

complete picture of how chemical species are distributed within a structured specimen such as a dilute biological tissue.

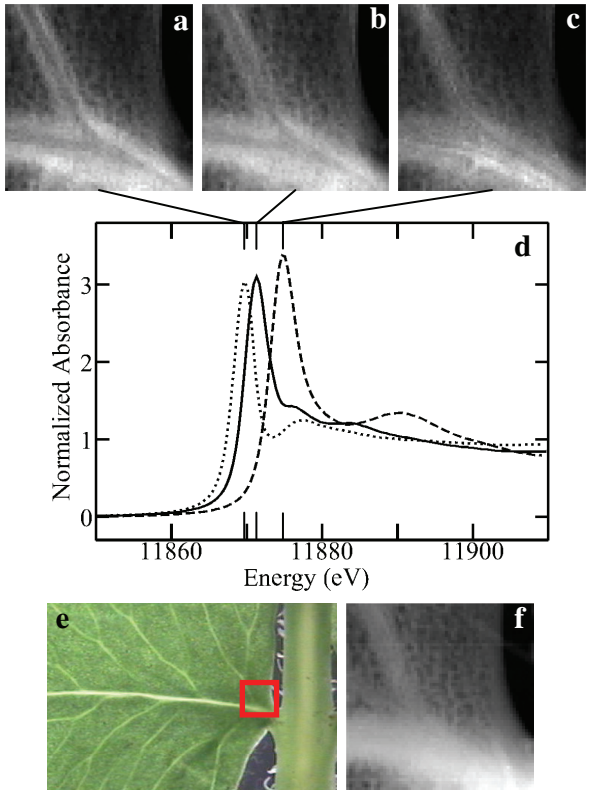

FIGURE 3. XAS imaging of arsenic in *Pteris vittata* fern. a-c show unconverted fluorescence maps recorded at three different incident energies a) 11869.8 eV, b) 11871.4 eV and c) 11874.8 eV. d) Bulk As K-edge spectra of solution species models. The incident energies of a-c) are identified in d) by vertical lines and are tuned for a) arsenic^{III}-thiolate (spectrum shown as dotted line), b) arsenite (solid) and c) arsenate (dashed). e) Optical micrograph identifying the imaged area. f) Thickness map in which the black to white intensity scale is 0 to 0.6 mm. The mid-vein and a minor vein of the sporophyte leaf can be seen. Scanned image is 600 µm x 600 µm with a pixel size of 10 µm.

Figure 3 shows an example of 3-component XAS imaging of a leaf blade of *Pteris vitatta*. Here, the incident energy was tuned for the peak of arsenate (Fig. 3c), arsenite (Fig. 3b) and arsenic^{III}-tris-thiolate (modeled as arsenic^{III}-tris-glutathione, Fig. 3a). These energies are identified on the spectra of Fig. 3d. It can be seen that at each energy more than one component is contributing to the fluorescence. As a consequence, the fluorescence images show considerable similarity (though some minor differences can be identified).

Figure 4 shows the processed images resulting from the fluorescence maps of Fig. 3. Figure 4 shows both the amounts (left hand column), and the concentrations (right hand column). The concentration is related to the amounts by dividing by the effective thicknesses (see Fig. 3f). Here, the maps for the three different chemical forms are seen to be very distinct. While the difference between the concentration and amounts images is not so distinct, factoring in the thickness does make a difference. For example, in the amounts map the arsenite appears to be at higher levels in the vein, but the concentration map shows that the opposite is true.

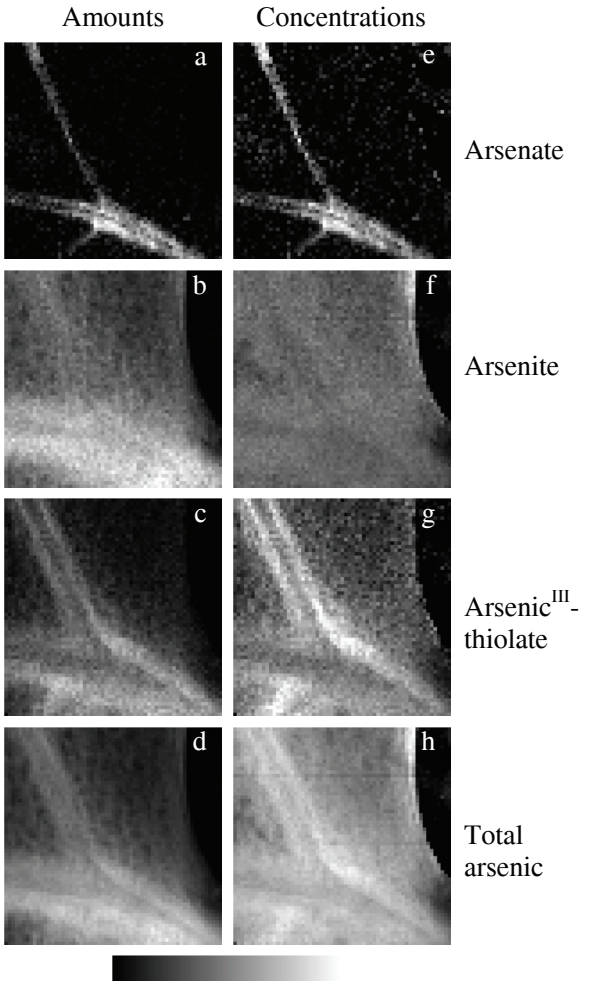

FIGURE 4. XAS images of arsenic species in *Pteris vittata* fern. Images are extracted from the data in Fig. 3. Left hand column shows quantitative maps of molar amounts per unit area, scaled in µmol.cm^{-2}. Right hand column shows the concentrations in mM. Intensities scale from zero (black) to maximum (white), with maxima as follows: a) 0.3, b) 1.0, c) 1.0 and d) 2.0 µmol.cm^{-2}; e) 6, f) 40 g) 20 and h) 40 mM. Scanned image is 600 µm x 600 µm with a pixel size of 10 µm.

Arsenate is present in a thin stream within the vein, and probably flowing within the xylem transport

vessels. Arsenite is present at high concentrations throughout the leaf, and arsenic^{III}-tris-thiolate is revealed as a highly localized sheaf around the vein. Other images [4] show that arsenate is transported from the roots to the leaves and converted in the blade. We speculate that these thiolate species may be implicated in the reduction of arsenate to arsenite. The arsenite is most likely stored in the vacuole [4].

A Viable Method for Biological Tissues

This example illustrates the strength of XAS imaging, versus the combination of μ-XRF and μ-XAS. As μ-XAS generally can be applied to a handful of spatial points, the detail of speciation in this case almost certainly would have remained obscure.

It is our experience that considerable chemical detail can be obtained even when μ-XAS spectra appear highly noisy and of poor quality. In these samples the noise is of course propagated to the images. However, the eye effectively integrates over the noise in the image to still pick out the structural details.

Despite the added time spent in collected the multiple images, the reward in terms of simultaneous spatial and chemical information is certainly worthwhile. With faster data processing, the time to scan one image should be considerably reduced, making this method more feasible. At present it has only been used for elements showing large spectroscopic changes (such as Se, S and As) but with adequate signal to noise it should in principal be feasible to distinguish chemical forms with less spectroscopic diversity. The more complete structural picture that it can yield, coupled with the significantly lower irradiation time, make this an attractive method for obtaining simultaneous chemical and spatial information from a dilute biological material.

ACKNOWLEDGMENTS

Both IJP and GNG are Canada Research Chairs at the University of Saskatchewan. We additionally gratefully acknowledge the Government of Saskatchewan, the Natural Sciences and Engineering Research Council of Canada, the Canadian Institutes of Health Research and the National Institutes of Health (USA). We are grateful to many colleagues with whom we have collaborated in our work, particularly Roger Prince (ExxonMobil BioMedical Sciences Inc) and Greg Hirsch (Hirsch Scientific), together with present and past members of our research groups. Data collection was carried out at the Stanford Synchrotron Radiation Laboratory, a national user facility operated by Stanford University on behalf of the U.S. Department of Energy, Office of Basic Energy Sciences. The SSRL Structural Molecular Biology Program is supported by the Department of Energy, Office of Biological and Environmental Research, and by the National Institutes of Health, National Center for Research Resources, Biomedical Technology Program.

REFERENCES

1. H. H. Harris, I. J. Pickering and G. N. George, *Science*, **301**(5637), 1203 (2003).
2. I. J. Pickering, R. C. Prince, D. E. Salt and G. N. George, *Proc. Natl. Acad. Sci.USA* **97**, 10717-10722 (2000).
3. I. J. Pickering, G. Hirsch, R. C. Prince, E. Y. Yu, D. E. Salt and G. N. George, *J. Synch. Radiat.* **10**(3), 289-290 (2003).
4. I. J. Pickering, L. Gumaelius, H. H. Harris, R. C. Prince, G. Hirsch, J. A. Banks, D. E. Salt, G. N. George, *Environ. Sci Technol*. in the press (2006).
5. L. Q. Ma, K. M. Komar, C. Tu, W. Zhang, Y. Cai and E. D. Kennelley, *Nature* **409**, 579 (2001).
6. S. M. Webb, J.-F. Gaillard, L. Q. Ma, C. Tu, *Environ. Sci. Technol.* **37**, 754 (2003).
7. J. W. Huang, C. Y. Poynton, L. V. Kochian, and M. P. Elless, *Environ. Sci. Technol*. **38**(12), 3412-3417 (2004).